Chemical Science

EDGE ARTICLE

View Article Online
View Journal | View Issue

Cite this: *Chem. Sci.*, 2018, **9**, 2609

Understanding light-driven H_2 evolution through the electronic tuning of aminopyridine cobalt complexes†

Arnau Call, [a] Federico Franco,[a] Noufal Kandoth, [a] Sergio Fernández, [a] María González-Béjar, [b] Julia Pérez-Prieto, [b] Josep M. Luis [c] and Julio Lloret-Fillol *[ad]

Received 5th October 2017
Accepted 18th December 2017

DOI: 10.1039/c7sc04328g

rsc.li/chemical-science

A new family of cobalt complexes with the general formula $[Co^{II}(OTf)_2(^{Y,X}Py^{Me}tacn)]$ ($\mathbf{1}^{R}$, $^{Y,X}Py^{Me}tacn$ = 1-[(4-X-3,5-Y-2-pyridyl)methyl]-4,7-dimethyl-1,4,7-triazacyclononane, (X = CN ($\mathbf{1}^{CN}$), CO_2Et ($\mathbf{1}^{CO2Et}$), Cl ($\mathbf{1}^{Cl}$), H ($\mathbf{1}^{H}$), NMe_2 ($\mathbf{1}^{NMe2}$)) where (Y = H, and X = OMe when Y = Me ($\mathbf{1}^{DMM}$)) is reported. We found that the electronic tuning of the $^{Y,X}Py^{Me}tacn$ ligand not only has an impact on the electronic and structural properties of the metal center, but also allows for a systematic water-reduction-catalytic control. In particular, the increase of the electron-withdrawing character of the pyridine moiety promotes a 20-fold enhancement of the catalytic outcome. By UV-Vis spectroscopy, luminescence quenching studies and Transient Absorption Spectroscopy (TAS), we have studied the direct reaction of the photogenerated $[Ir^{III}(ppy)_2(bpy^{\bullet-})]$ ($\mathbf{PS}_{Ir}$) species to form the elusive Co^{I} intermediates. In particular, our attention is focused on the effect of the ligand architecture in this elemental step of the catalytic mechanism. Finally, kinetic isotopic experiments together with DFT calculations provide complementary information about the rate-determining step of the catalytic cycle.

Introduction

Hydrogen production by artificial photosynthesis is one of the most promising technologies to provide a clean and sustainable carbon-free fuel and feedstock for innumerable chemical processes.[1] Better understanding of the mechanisms for H_2 evolution is needed to develop more efficient catalysts. In this regard, a plethora of molecular catalysts based on Mo, Fe, Co and Ni have been studied as model systems.[2] However, the challenging characterization of the key intermediates and the intrinsic complexity of the catalytic mechanisms enormously hinders their elucidation.[3] In this regard, aminopyridine cobalt complexes are promising platforms to get insights into the elemental steps of the H_2 evolution mechanism.

The commonly proposed mechanism for water reduction catalysed by aminopyridine cobalt complexes involves the formation of a low oxidation state (presumably Co^{I}), followed by protonation. Further reduction and protonation steps are invoked to induce the H–H bond formation (Scheme 1).[4] However, it is not well understood how $Co^{II/I}$ reduction potential and cobalt hydride pK_a values actually affect the overall reaction rate.[5] On the other hand, although many studies have been focused on the detection of the short-lived Co^{I} species,[4b,d,6] to the best of our knowledge the direct reaction of Co^{II} complexes with a reduced state of the photosensitizer still remains undefined.[7] Likewise, the influence of the electronic effects of the ligand on the overall catalytic rate of the process is not fully understood.[4b,c]

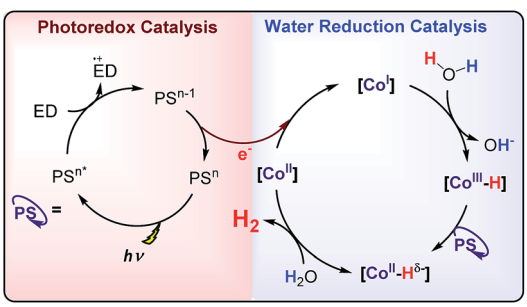

Scheme 1 Commonly proposed mechanism for light-driven water reduction by aminopyridine cobalt complexes.

[a]*Institute of Chemical Research of Catalonia (ICIQ), The Barcelona Institute of Science and Technology, Avinguda Països Catalans 16, 43007 Tarragona, Spain. E-mail: jlloret@iciq.es*

[b]*Instituto de Ciencia Molecular (ICMol), Universidad de Valencia, C/Catedrático José Beltrán 2, Paterna, E46980 Valencia, Spain*

[c]*Institut de Química Computacional i Catàlisi (IQCC), Departament de Química, Universitat de Girona, Campus Montilivi, E17071 Girona, Catalonia, Spain*

[d]*Catalan Institution for Research and Advanced Studies (ICREA), Passeig Lluïs Companys, 23, 08010, Barcelona, Spain*

† Electronic supplementary information (ESI) available. CCDC 1578284–1578289. For ESI and crystallographic data in CIF or other electronic format see DOI: 10.1039/c7sc04328g

Electronic effects have often been explored to gain insight into the hydrogen evolution catalytic mechanisms (Fig. 1).[5,8] However, the studies are limited by the capacity of ligand modification, and the stability or activity of the water reduction catalysts under study. In many cases, this restricts or even leads to contradictory conclusions. For instance, for the [Co(R-PY5Me$_2$)(H$_2$O)](OTf)$_2$ series (R = p-CF$_3$ (2), p-H (3), p-NMe$_2$ (4)), the photo- and electrocatalytic activity for H$_2$ evolution was enhanced by introducing the electron withdrawing CF$_3$ group.[9] In contrast, for complexes [Co(bpy(Py-R)$_2$Me)(X)(Y)](OTf) (R = p-CF$_3$ (5), p-H (6), X, Y = CH$_3$CN or OTf) and [Co((bpy)$_2$PyMe-R(OTf))](OTf) (R = p-CF$_3$ (7), p-H (8)), the introduction of a CF$_3$ group led to a lower catalytic activity.[10] In the case of cobalt corroles (H, F, Cl and Br, (9–12)) the decrease of the electron density over the metal centre induces an increase of the electrocatalytic activity.[11]

With the aim to shed light on the key factors controlling the photocatalytic water reduction activity, we have developed a new family of well-defined cobalt complexes that are highly active in light-driven water reduction and whose electronic features can be tuned. To this end, we explored the cobalt complexes obtained from the readily available 1-[(4-X-3,5-Y-2-pyridyl)methyl]-4,7-dimethyl-1,4,7-triazacyclononane (^{Y,X}Py^{Me}tacn) ligand family. In addition, we previously found that similar coordination complexes are water stable under reductive conditions and highly chelating.[7,12] The electronic properties of the ^{Y,X}Py^{Me}tacn ligand are easily and systematically tuned by the substitution at the γ- (X: CN ($\mathbf{1}^{CN}$), CO$_2$Et ($\mathbf{1}^{CO2Et}$), Cl ($\mathbf{1}^{Cl}$), H ($\mathbf{1}^{H}$), NMe$_2$ ($\mathbf{1}^{NMe2}$)) and β-positions (X: OMe when Y: Me ($\mathbf{1}^{DMM}$)) of the pyridine (Scheme 2).[12d]

Herein, we report the synthesis, characterisation and photocatalytic water reduction activity of this new family of cobalt complexes with the general formula [Co^{II}(OTf)$_2$(^{Y,X}Py^{Me}tacn)]. We present a detailed mechanistic study to elucidate the key steps of the H$_2$ formation and how the electronic nature of the ligand affects the total reaction rate. We also study the role of [Ir^{III}(ppy)$_2$(bpy)]PF$_6$ ($\mathbf{PS_{Ir}}^+$), its reduction to [Ir^{III}(ppy)$_2$(bpy$^{\bullet-}$)] ($\mathbf{PS_{Ir}}$) and the reaction of the latter with the cobalt catalysts to form Co^{I} species by steady state and transient absorption kinetics and fluorescence quenching experiments. Deuterium labelling and computational modelling also provided complementary information about the rate-determining step of the catalytic cycle. Altogether, these data allow for the rationalisation of the light-driven H$_2$ evolution mechanism by $\mathbf{1}^{R}$ catalysts in terms of the electronic effects. We envision that the provided information will be valuable to design future generations of water reduction catalysts.

Results and discussion

Synthesis and characterization

The ^{Y,X}Py^{Me}tacn (X ≠ CN) ligands were synthesised according to the literature (Scheme 2)[12b,d] and the ^{H,CN}Py^{Me}tacn ligand was obtained following an equivalent synthesis (see ESI Section 4.1†). An equimolar reaction of ^{Y,X}Py^{Me}tacn with [Co^{II}(OTf)$_2$-(MeCN)$_2$] gave six well-defined Co^{II} complexes ($\mathbf{1}^{R}$) as crystalline materials in goods yields (61–86%). All complexes were fully characterized by UV-Vis absorption spectroscopy, ESI-MS, FT-IR, cyclic voltammetry, elemental analysis, ^{1}H-NMR and single crystal X-ray diffraction crystallography (see ESI Section 4† for details). The ^{1}H-NMR spectra window for $\mathbf{1}^{R}$ complexes ranged from −14 to 240 ppm and followed the Curie's law, which is in

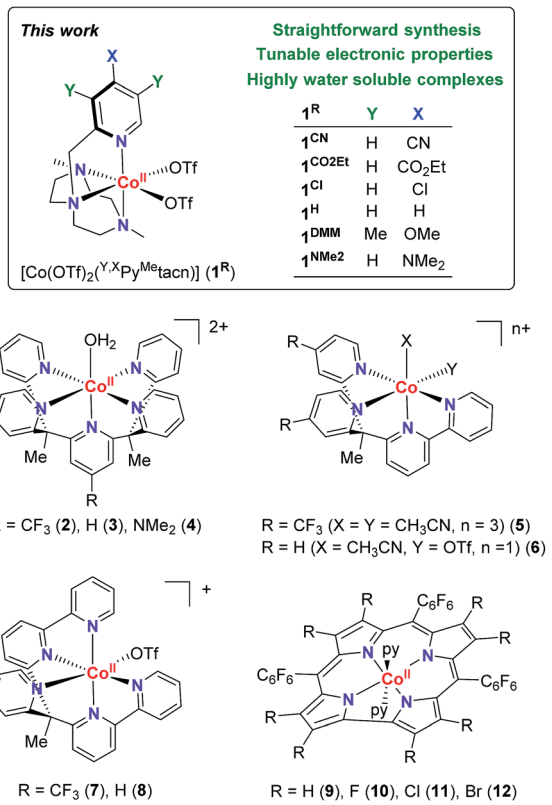

$\mathbf{1}^{R}$	Y	X
$\mathbf{1}^{CN}$	H	CN
$\mathbf{1}^{CO2Et}$	H	CO_2Et
$\mathbf{1}^{Cl}$	H	Cl
$\mathbf{1}^{H}$	H	H
$\mathbf{1}^{DMM}$	Me	OMe
$\mathbf{1}^{NMe2}$	H	NMe_2

Fig. 1 (Top) Cobalt complexes developed for this study. (Bottom) Selected cobalt water reduction catalysts where electronic effects have been reported in literature.

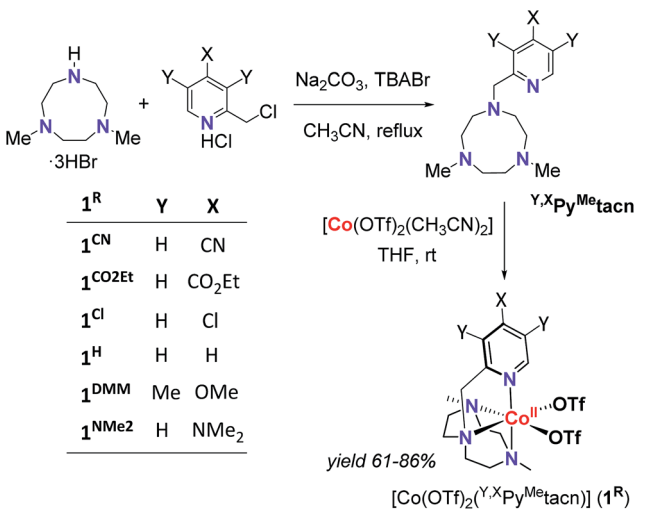

$\mathbf{1}^{R}$	Y	X
$\mathbf{1}^{CN}$	H	CN
$\mathbf{1}^{CO2Et}$	H	CO_2Et
$\mathbf{1}^{Cl}$	H	Cl
$\mathbf{1}^{H}$	H	H
$\mathbf{1}^{DMM}$	Me	OMe
$\mathbf{1}^{NMe2}$	H	NMe_2

Scheme 2 General scheme for the straightforward preparation of ligands and complexes studied herein.

agreement with a high spin ($S = 3/2$) d^7 Co^{II} paramagnetic species. A down-shift of the α-proton of the pyridine, while increasing the electron withdrawing character of the ligand, clearly indicates the ligand influence in the physical properties of the complex (see ESI Section 4.2.2†).

The solid-state structures of the synthesised cobalt complexes show slightly distorted octahedral coordination geometries for the Co^{II} centre with four coordination sites occupied by the three N atoms of the tacn moiety and the N atom of the pyridine (Fig. 2), respectively, being isostructural to the previously reported equivalent Fe^{II} complexes.[12d] The Co–N bond lengths ranges from 2.0 to 2.2 Å, matching well with reported $S = 3/2$ Co^{II} complexes.[10a,13] The electronic properties of the substituted pyridine are reflected in a systematic modification of the Co^{II} coordinative environment. For instance, the Co–N_{py} bond length (d(Co–N_{py})) becomes smaller upon increasing the electron-donating character of the substituent (Fig. 2, Tables S1–S4†).

Both, X-ray diffraction and paramagnetic ^{1}H-NMR data clearly show that the nature of the pyridine substituents significantly alters the Py–cobalt interaction in a systematic manner.

Reduction potentials. Cyclic Voltammetry (CV) was carried out in dry CH_3CN under inert (Ar) atmosphere for all $\mathbf{1^R}$ complexes, showing the $Co^{III/II}$ and $Co^{II/I}$ events (Fig. 3, left). The $Co^{III/II}$ features appeared to be quasi-reversible with a large ΔE_p (~300–500 mV), which is commonly related to the transition from high-spin Co^{II} to low-spin Co^{III}, presumably accompanied by relevant structural changes.[10b] The good linear correlation between the $E_{1/2}(Co^{III/II})$ values and the Hammett parameters (σ) reflects a direct dependence of the $Co^{III/II}$ redox potential on the electronic effects of the substituents introduced at the pyridine ligand (Fig. 3, right, triangles).[14]

In a similar manner, the $E_{1/2}(Co^{II/I})$ values provide a good linearity in the Hammett plot ($E_{1/2}(Co^{II/I})$ *vs.* σ (Fig. 3)), and an overall anodic shift of ~380 mV from $\mathbf{1^{NMe2}}$ to $\mathbf{1^{CN}}$ in the series (Table 1) is observed. Electron-withdrawing groups at the *para* position of pyridine lead to reversible $Co^{II/I}$ waves, providing experimental $E_{1/2}(Co^{II/I})$ values of −1.53 V and −1.44 V (*vs.* $Fc^{+/0}$) for $\mathbf{1^{CO2Et}}$ and $\mathbf{1^{CN}}$, respectively. In contrast, in the case of $\mathbf{1^{Cl}}$, $\mathbf{1^{H}}$, $\mathbf{1^{DMM}}$ and $\mathbf{1^{NMe2}}$, the $Co^{II/I}$ reduction appears as an irreversible peak at 0.1 V s^{-1}, with a small oxidative peak occurring at *ca.* 550 mV more positive. However, reversibility of $Co^{II/I}$ wave is found at higher scan rates (Fig. S14–S17†). A linear dependence of the $Co^{II/I}$ peak current (i_p) with the square root of the scan rate for all the $\mathbf{1^R}$ complexes is indicative of a diffusion-controlled reduction process (Fig. S14–S19†).

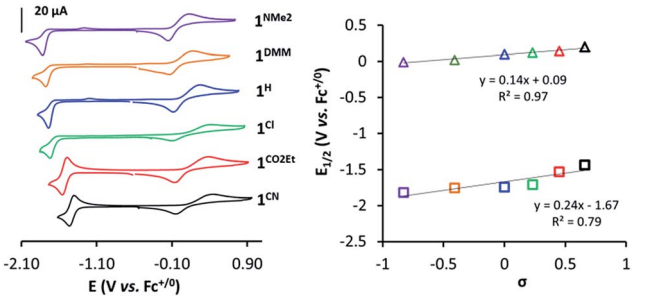

Fig. 3 CVs of $\mathbf{1^R}$ (1 mM) in $TBAPF_6$/MeCN (0.1 M) at $v = 100$ mV s^{-1} under Ar (Left). Plot of $E_{1/2}(Co^{III/II})$ (triangles) and $E_{1/2}(Co^{II/I})$ (squares) *vs.* Hammett parameter (σ) (Right). Labels: $\mathbf{1^{CN}}$ (black), $\mathbf{1^{CO2Et}}$ (red), $\mathbf{1^{Cl}}$ (green), $\mathbf{1^{H}}$ (blue), $\mathbf{1^{DMM}}$ (orange), $\mathbf{1^{NMe2}}$ (purple).

Photocatalytic water reduction

Light-driven H_2 evolution studies were performed to explore the influence of the ligand substitution on the catalytic activity of $\mathbf{1^R}$ complexes. We employed $[Ir^{III}(ppy)_2(bpy)](PF_6)$ ($\mathbf{PS_{Ir}^+}$) as photosensitiser and Et_3N as sacrificial electron donor in MeCN : H_2O (4 : 6) solvent mixture to guarantee the solubility of all components and irradiated at $\lambda = 447 \pm 20$ nm ($T = 25$ °C). The gas evolution was monitored and H_2 quantified by gas-chromatography (GC-TCD). Control experiments showed that all components are necessary for H_2 formation and only a negligible amount of H_2 was detected using $[Co^{II}(OTf)_2(MeCN)_2]$ as catalyst. The amount of H_2 produced and the rate were unaffected in Hg^0 poisoning experiments (1000 eq., see Fig. S20†), suggesting molecular catalysis,[15] in concordance with the absence of induction time.

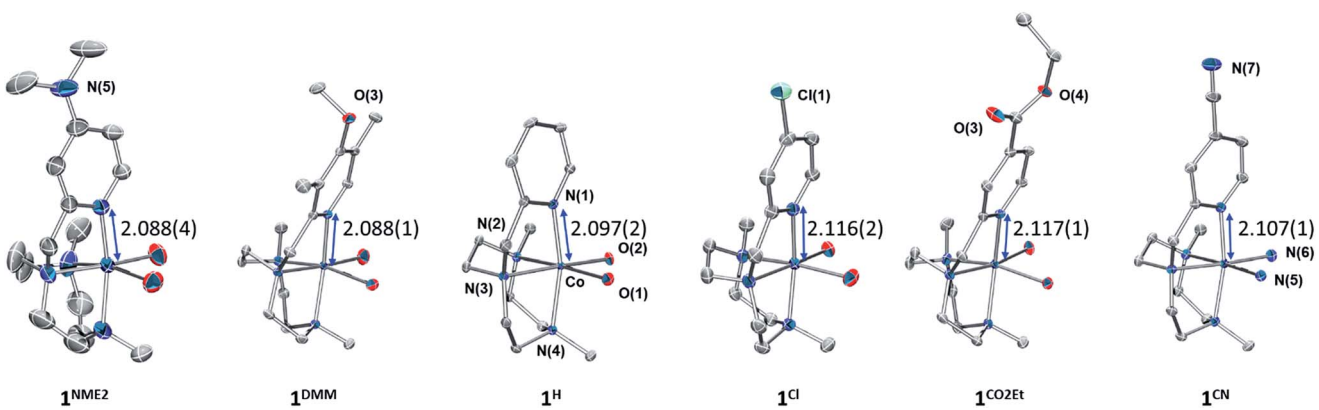

Fig. 2 Thermal ellipsoid plots of $\mathbf{1^{NMe2}}$ (30% probability) and $\mathbf{1^{CN}}$, $\mathbf{1^{CO2Et}}$, $\mathbf{1^{Cl}}$, $\mathbf{1^{H}}$, $\mathbf{1^{DMM}}$ (50% probability). Triflate ions and acetonitrile molecules bonded to the cobalt centre, as well as solvent molecules and hydrogen atoms are omitted for clarity. The Co–N_{py} bond lengths are given in Å.

Table 1 Experimental $Co^{III/II}$ and $Co^{II/I}$ reduction potentials and light-driven H_2 production for $\mathbf{1^R}$

Complex	$E_{1/2}$[a] ($Co^{III/II}$) (V)	$E_{1/2}$[a] ($Co^{II/I}$) (V)	H_2 (mmol)	Rate[e] (mmol H_2 h^{-1})	Φ[g] (%)
$\mathbf{1^{NMe2}}$	−0.01	−1.82[b]	0.013 ± 0.002	0.025 ± 0.002	0.7 ± 0.1
$\mathbf{1^{DMM}}$	+0.02	−1.76[c]	0.018 ± 0.001	0.071 ± 0.003	1.9 ± 0.2
$\mathbf{1^{H}}$	+0.10	−1.74[b]	0.042 ± 0.002	0.137 ± 0.002	3.7 ± 0.4
$\mathbf{1^{Cl}}$	+0.12	−1.71[d]	0.051 ± 0.005	0.170 ± 0.009	4.6 ± 0.5
$\mathbf{1^{CO2Et}}$	+0.14	−1.53	0.25 ± 0.01	0.356 ± 0.007	9.7 ± 1.0
$\mathbf{1^{CN}}$	+0.20	−1.44	0.21 ± 0.01	0.336 ± 0.001	9.1 ± 0.9
$\mathbf{PSIr^{+/0}}$		−1.77[f]			

[a] $E_{1/2}$ *vs.* $Fc^{+/0}$. [b] At $v = 50$ V s^{-1}. [c] At $v = 20$ V s^{-1}. [d] At $v = 10$ V s^{-1}. [e] Measured before 10% H_2 formed. Experimental conditions: $\mathbf{1^R}$ (50 μM), $\mathbf{PS_{Ir}}$ (150 μM) in CH_3CN : H_2O : Et_3N (4 : 6:0.2 mL), irradiation (λ = 447 nm) at 25 °C. [f] Reduction potential of the iridium photosensitizer ($\mathbf{PS_{Ir}^{+/0}}$) *vs.* $Fc^{+/0}$ under catalytic conditions. [g] Calculated as $\Phi = 2\times n(H_2)/(n(\text{photons})) \times 100$.

All $\mathbf{1^R}$ catalysts were active for the photo-induced hydrogen evolution but highly dependent on the substituent at the pyridine, following the order $\mathbf{1^{NMe2}} < \mathbf{1^{DMM}} < \mathbf{1^{H}} < \mathbf{1^{Cl}} < \mathbf{1^{CO2Et}} \sim \mathbf{1^{CN}}$. Indeed, the catalytic rate increases with the electron-withdrawing character of the ligand, in agreement with the $E_{1/2}(Co^{II/I})$ value (Table 1). Under standard conditions, the catalytic rate for the most active catalyst, $\mathbf{1^{CO2Et}}$, was about 14-fold higher than $\mathbf{1^{NMe2}}$ (the least active in the series), producing around 20 times more H_2 (initial rate (v_i) is 0.356 *vs.* 0.025 mmol h^{-1} and 6.1 *vs.* 0.3 mL H_2, respectively) (Table 1, Fig. 4 left/middle). Interestingly, the hydrogen evolution rate ($\log(v_i(\mathbf{1^R})/v_i(\mathbf{1^H}))$ correlates very well with the sigma Hammett parameters (Fig. 4 right), but also with the redox $E_{1/2}(Co^{II/I})$ values (Fig. S21†). We have also calculated quantum yields for the photocatalytic water reduction, (Φ, based on two photons absorbed per produced H_2 molecule), improving from 0.7% to 9.7% in the series from $\mathbf{1^{NMe2}}$ to $\mathbf{1^{CO2Et}}$ (see Table 1).

Since the $\mathbf{1^{CO2Et}}$ is the most active complex of the series, next we optimised its catalytic activity *versus* catalyst concentration. A non-linear increase of the total amount of H_2 produced was observed upon increasing the amount of catalyst from 0.25 to 100 μM (Fig. S22†). This is in agreement with previous studies on aminopyridine cobalt complexes.[16] Under optimised conditions, we obtained a TON value of about 9000 and TOF_{max} > 52 000 h^{-1} at 0.25 μM catalyst (Fig. 5). To the best of our knowledge, the TOF_{max} value for $\mathbf{1^{CO2Et}}$ is higher than the highest reported to date for light-driven H_2 evolution catalysts based on polypyridyl ligands.[17] Among the latter, a TOF_{max} of 5880 h^{-1} and TON of *ca.* 33 300 were reported by Alberto *et al.* for the [CoBr(aPPy)]Br (aPPy = Di-2,2′-bipyridiyl-6-yl(pyridin-2-yl)methanol) complex after 70 h of irradiation.[18] Nevertheless, we favour a TOF analysis rather that total TON measured on the plateau, since the TOF better represent electronic effects in the mechanism and the TON combines rate and stability. On the other hand, the water reduction quantum yield (Φ) for $\mathbf{1^{CO2Et}}$ (9.7% ± 1.0) is comparable to the highest reported value (7.5% ± 0.8)[19] for similar Co complexes.[19,20]

Mechanistic investigations

The intriguing electronic effects observed and the high catalytic activity of $\mathbf{1^{CO2Et}}$ and $\mathbf{1^{CN}}$ aimed us to study the mechanism in detail. Analysis of the catalytic experiments shows that the hydrogen evolution (at 10% of H_2 formed) has a first-order dependence on $\mathbf{1^{CO2Et}}$ at concentrations below 2.5 μM (Fig. 5, right). Therefore, we propose that the catalytic mechanism is single site and follows a heterolytic H–H bond formation. At higher cobalt concentrations (in the range 2.5–100 μM) a saturation of the initial rate is observed. This might suggest that the catalytic cycle is controlled by the photon-flux or/and by the regeneration of the active Co^{I} species, *via* Co^{II} + $\mathbf{PS_{Ir}}$ ⇆ Co^{I} + $\mathbf{PS_{Ir}}^{+}$ ($\mathbf{PS_{Ir}}$ = $Ir^{III}(ppy)_2(bpy^{\bullet-})$) pre-equilibrium. The latter possibility is further supported by the direct reaction of *in situ*

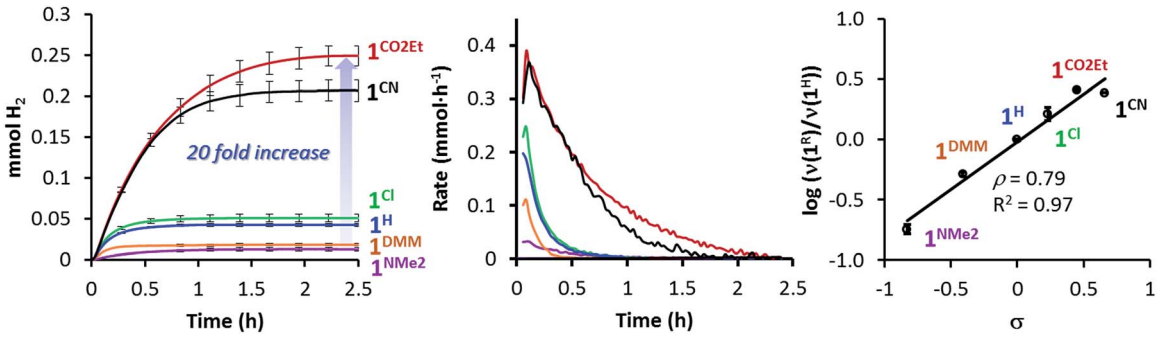

Fig. 4 On-line traces and rates of H_2 formed *vs.* time for $\mathbf{1^R}$ complexes (Left and Middle, respectively). Conditions: $\mathbf{1^R}$ (50 μM) and $\mathbf{PS_{Ir}}^{+}$ (150 μM) in CH_3CN : H_2O : Et_3N (4 : 6:0.2 mL) irradiated (λ = 447 nm) at 25 °C. (Right) Hammett plot of $\log(v(\mathbf{1^R})/v(\mathbf{1^H}))$ (at 10% conversion) *vs.* the σ Hammett value. $\mathbf{1^{CN}}$ (black), $\mathbf{1^{CO2Et}}$ (red), $\mathbf{1^{Cl}}$ (green), $\mathbf{1^{H}}$ (blue), $\mathbf{1^{DMM}}$ (orange) and $\mathbf{1^{NMe2}}$ (purple).

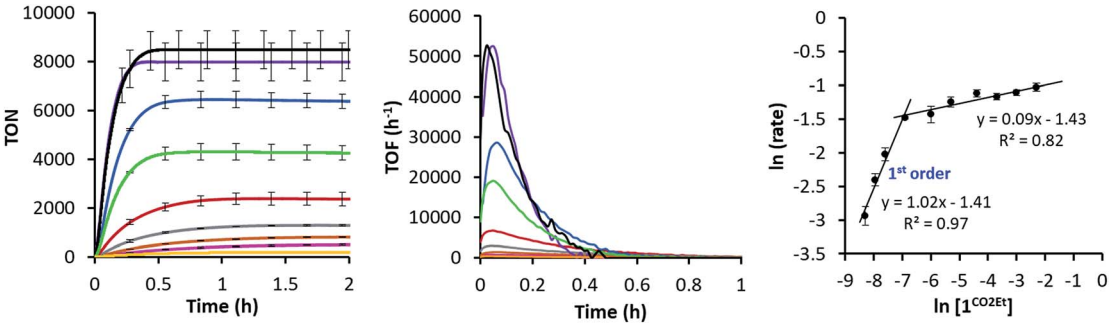

Fig. 5 (Left) Dependence of the H_2 evolution with the concentration of $\mathbf{1}^{CO2Et}$ (100 μM, yellow; 50 μM, pink; 25 μM, orange; 12.5 μM, grey; 5 μM, red; 2.5 μM, green; 1 μM, blue; 0.5 μM, purple; 0.25 μM, black). (Middle) On-line H_2 evolved traces and rates *vs.* time at different concentrations of $\mathbf{1}^{CO2Et}$ (0.25–100 μM). Conditions: $\mathbf{PS_{Ir}}^+$ (150 μM) in CH_3CN : H_2O : Et_3N (4 : 6:0.2 mL) irradiated (λ = 447 nm) at 25 °C. (Right) Logarithmic plot of catalytic rate as a function of $\mathbf{1}^{CO2Et}$ concentration.

formed $[Ir^{III}(ppy)_2(bpy^{\bullet-})]$ with $\mathbf{1^R}$. Subsequent reactivity studies have been performed under relevant conditions for catalysis.

Reactivity of the $[Ir^{III}(ppy)_2(bpy)]^+$ ($\mathbf{PS_{Ir}}^+$) excited state ($^*\mathbf{PS_{Ir}}^+$). Steady-state and time-resolved luminescence quenching studies. In order to understand the reactivity of $^*\mathbf{PS_{Ir}}^+$, steady state and time-resolved (single photon counting) luminescence studies were carried out by titration with both $\mathbf{1^{CN}}$ and an electron donor (Et_3N) at concentrations relevant for catalysis in H_2O : CH_3CN (4 : 6). The emission spectra and the lifetime decay of $^*\mathbf{PS_{Ir}}^+$ are practically unchanged upon addition of $\mathbf{1^{CN}}$ aliquots (Fig. S25†) while undergo quenching with Et_3N (Fig. S26A–C†). These results indicate that $^*\mathbf{PS_{Ir}}^+$ is predominantly quenched by the sacrificial tertiary amine (Et_3N). As a consequence, $\mathbf{PS_{Ir}}$ together with triethylamine radical cation are generated upon irradiation. Stern–Volmer quenching analysis for $^*\mathbf{PS_{Ir}}^+$ with Et_3N provided a linear fit for both the steady-state and time-resolved luminescence, with a quenching rate constant (k_q) of 1.7 × 10^7 M^{-1} s^{-1} and 1.9 × 10^7 M^{-1} s^{-1}, respectively (H_2O : CH_3CN (4 : 6), see ESI Table S6 and Fig. S26D†).[21]

***In situ* formation and reactivity of $\mathbf{PS_{Ir}}$ with $\mathbf{1^R}$.** We were interested in evaluating the reactivity of the reduced form of the $\mathbf{PS_{Ir}}^+$, $[Ir^{III}(ppy)_2(bpy^{\bullet-})]$ ($\mathbf{PS_{Ir}}$), with our cobalt complexes to form Co^I species. The isolation of $\mathbf{PS_{Ir}}$ is very challenging due to its high reactivity, and to our knowledge has not previously been reported.[22] Therefore, we studied the *in situ* formation of $\mathbf{PS_{Ir}}$ monitored by UV-Vis spectroscopy and its reaction with the different $\mathbf{1^R}$ catalysts in both pure CH_3CN and under photocatalytic H_2 evolution conditions.

Study of the $\mathbf{PS_{Ir}}$ formation and their reactivity with $\mathbf{1^R}$ in pure CH_3CN. The study in pure acetonitrile allows for a model study of the reactivity between $\mathbf{1^R}$ and the reduced form of the photoredox catalyst. This is the first step of the catalytic cycle, which is difficult to study otherwise. Optimum conditions to study the formation of $\mathbf{PS_{Ir}}$ consist in the irradiation (λ = 447 nm) of a solution containing $\mathbf{PS_{Ir}}^+$ (0.1 mM) and Et_3N (1000 eq.) in anhydrous degassed CH_3CN under N_2 atmosphere at −20 °C, which produced the appearance of three new UV-Vis bands at 385, 495 and 523 nm and a broad band centred at 850 nm consistent with an electron delocalized over the bpy ligand (Fig. 6, iia). These new bands are ascribed to the formation of $\mathbf{PS_{Ir}}$.[7] The UV-Vis spectra recorded during irradiation (ESI Section 3† for the Experimental setup) showed a fast formation of $\mathbf{PS_{Ir}}$ up to a plateau (*ca.* 30 s), followed by a slow decay (Fig. S31†).[22] Interestingly, the addition of $\mathbf{1^{CN}}$ (0.2 eq., 20 μM) at the maximized $\mathbf{PS_{Ir}}$ absorbance (527 nm), led to an instantaneous disappearance (mixing time) of the $\mathbf{PS_{Ir}}$ spectral features. This is in agreement with a fast electron transfer from the $\mathbf{PS_{Ir}}$ to $\mathbf{1^{CN}}$ that leads to the formation of a new reduced cobalt species (presumably Co^I), regenerating $\mathbf{PS_{Ir}}^+$ (Fig. 6 (i and iib)). Interestingly, the amount of $\mathbf{PS_{Ir}}$ vanished is proportional to the amount of $\mathbf{1^{CN}}$ added. $\mathbf{PS_{Ir}}$ was fully consumed for a $[\mathbf{1^{CN}}]$ equal or higher than 15 μM. Considering an ideal 1 : 1 stoichiometric reaction between $\mathbf{PS_{Ir}}$ and $\mathbf{1^{CN}}$, the estimated *in situ* photogenerated $\mathbf{PS_{Ir}}$ is *ca.* 15 μM, the 15% of the initial $[\mathbf{PS_{Ir}}^+]$ (Fig. S27 and S28†). Further irradiation partially recovered the UV-Vis bands belonging to $\mathbf{PS_{Ir}}$ (Fig. 6 (iic)). Analogous studies with different $\mathbf{1^R}$ complexes showed that the extension of the $\mathbf{PS_{Ir}}$ decay depends on the reduction potential of $\mathbf{1^R}$, following the same trend observed for the photocatalytic H_2 evolution $\mathbf{1^{CN}}$ – $\mathbf{1^{CO2Et}}$ > $\mathbf{1^{Cl}}$ > $\mathbf{1^{H}}$ > $\mathbf{1^{DMM}}$ > $\mathbf{1^{NMe2}}$ (Fig. S29 and S30†).[23]

In addition, changes in absorbance of $\mathbf{PS_{Ir}}$ at 527 nm and the difference between $E_{1/2}(Co^{II/I})$ and $E_{1/2}(Ir^{+/0})$ (−1.76 V *vs.* $Fc^{+/0}$) reduction potential follows the Nernst equation (eqn (S3) and (S4), see ESI† for details), reproducing well the sigmoidal theoretical curve (Fig. 7). It is important to notice that a similar dependence is observed with H_2 evolution initial rates measured under the catalytic conditions. These data suggest that the H_2 evolution rate, catalysed by the $\mathbf{1^R}$ complexes, is mainly controlled by the redox potential of the $Co^{II/I}$ event.

Study of the formation of $\mathbf{PS_{Ir}}$ and reactivity with $\mathbf{1^R}$ under catalytic conditions. Similar absorption kinetics experiments were carried out by using MeCN : H_2O (2 : 3) mixture as solvent. The reactivity of the $\mathbf{PS_{Ir}}$ with $\mathbf{1^R}$ complexes under catalytic conditions is similar to that observed in dry CH_3CN. We monitored at the same time UV-Vis spectral changes and the amount of evolved H_2 during the reaction. In a typical experiment, 0.1 eq. of $\mathbf{1^R}$ catalysts were added to a MeCN : H_2O (0.8 : 1.2 mL) solution containing $\mathbf{PS_{Ir}}^+$ (0.25 mM) and Et_3N (100 mM) under N_2 atmosphere at 25 °C. *In situ* produced $\mathbf{PS_{Ir}}$ rapidly

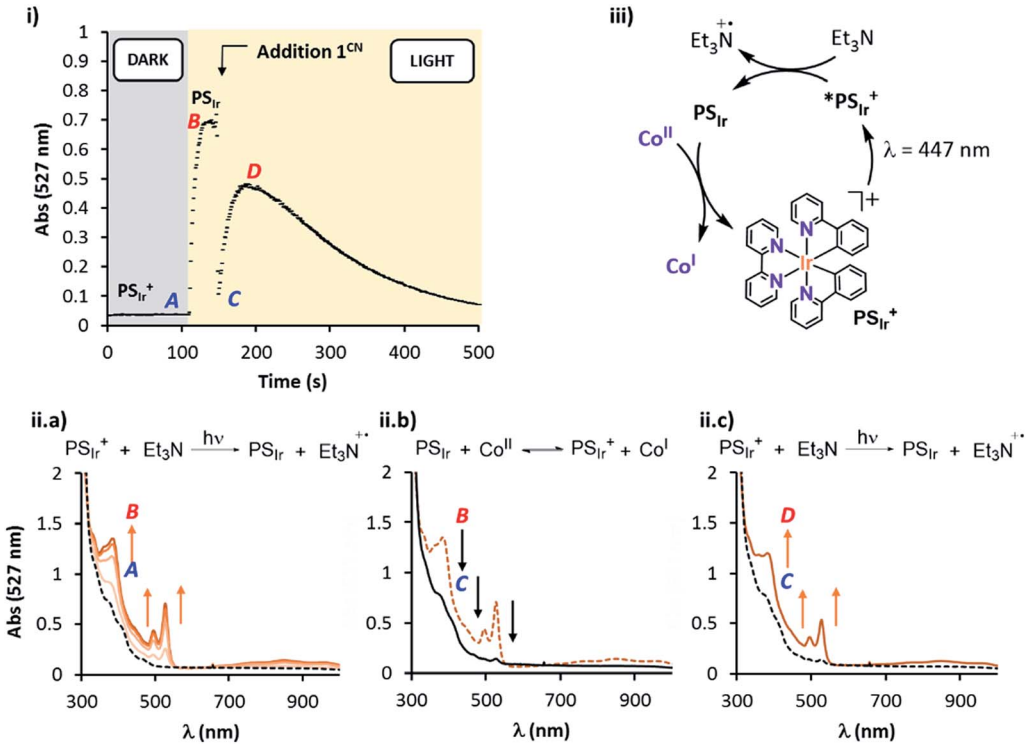

Fig. 6 Titration studies of PS_{Ir}^{+} (100 μM) by addition of $\mathbf{1}^{CN}$ (15 μM) in the presence of Et_3N (1000 eq.) in acetonitrile at −20 °C and irradiated at 447 nm. (i) UV-Vis traces at 527 nm and the corresponding evolution of their UV-Vis spectra, (A) switch on the irradiation at 447 nm, (B) maximized absorbance at 527 nm, (C) after 1 s of $\mathbf{1}^{CN}$ (1 eq., 15 μM) addition (D) maximum regeneration of PS_{Ir} under continuous irradiation. (ii.a) from PS_{Ir}^{+} to PS_{Ir} (30 s of irradiation), (ii.b) after addition of $\mathbf{1}^{CN}$ (1 eq., 15 μM) and (ii.c) regeneration of PS_{Ir} under continuous irradiation. (iii) Proposed catalytic mechanism.

decayed upon the addition of $\mathbf{1}^{R}$ under continuous light irradiation (λ = 447 nm).[24] The extent and rate of such decay depends on the $Co^{II/I}$ redox potential of the added $\mathbf{1}^{R}$ catalyst, being faster for the more electron-poor $\mathbf{1}^{R}$ complexes (Fig. 7). The resulting order, $\mathbf{1}^{CO2Et} > \mathbf{1}^{Cl} > \mathbf{1}^{H} > \mathbf{1}^{DMM} > \mathbf{1}^{NMe2}$, qualitatively reproduces well the rate for H_2 formation and is fully consistent with the results in anhydrous CH_3CN (Fig. 8). It is worth noting that no H_2 was detected neither under irradiation of PS_{Ir}^{+} in absence of catalyst nor under dark conditions.

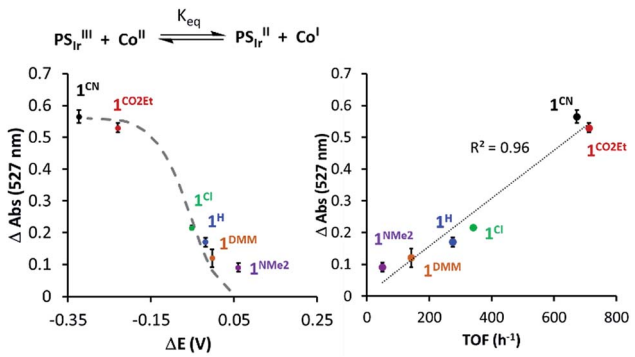

Fig. 7 (Left) The 527 nm absorbance decay upon addition of $\mathbf{1}^{R}$ *vs.* $\Delta(E_{1/2}(PS_{Ir}^{+}/PS_{Ir}) - E_{1/2}(Co^{II/I}))$. (Right) 527 nm absorbance of PS_{Ir} decay upon addition of $\mathbf{1}^{R}$ *vs.* TOF (h^{-1}) (initial rate at 10% conversion of H_2 evolution). The dashed grey line refers to the theoretical values predicted from Nernst equation (see Section ESI 6.1†).

Study of the PS_{Ir} reactivity with $\mathbf{1}^{CO2Et}$ by transient absorption spectroscopy (TAS). Nanosecond transient absorption spectroscopy was used in order to achieve further mechanistic understanding on the PS_{Ir} formation and subsequent generation of Co^{I} in neat acetonitrile.

First, the PS_{Ir}^{+} (50 μM) excitation (λ_{ex} = 355 nm laser pulse) (see ESI† Experimental section) led to a strong characteristic emission centred at 600 nm and a positive band below 490 nm due to the formation of MLCT and LC PS_{Ir}^{+} triplet bands, both λ_{max} (600, 470 nm) having a lifetime of *ca.* 350 ns (Fig. S32†). The differential absorption spectra and lifetime are in agreement with the reported excited triplet state ($^{3}PS_{Ir}^{+}$).[25] The Et_3N titration was followed at 600 nm and afforded a bimolecular quenching rate constant (k_q) of 2.5 × 10^{8} M^{-1} s^{-1} (Fig. S33, Table S7,† CH_3CN as solvent). Moreover, we studied the changes in the transient absorption spectra of PS_{Ir}^{+} (50 μM), Et_3N (20 mM) in presence of $\mathbf{1}^{CO2Et}$ (80 μM).

Interestingly, upon 355 nm laser excitation of a mixture containing PS_{Ir}^{+} (50 μM), Et_3N (20 mM) and $\mathbf{1}^{CO2Et}$ (80 μM) in degassed CH_3CN under Ar, a new transient species was detected (Fig. 9), presumably Co^{I},[26] which has two absorption bands centred at 390 and 510 nm. The kinetic profile at 500 nm shows an estimate rise-time of *ca.* 1 μs for the generation of Co^{I} species (Fig. S34†). Since the rate constant of the electron transfer from PS_{Ir} to Co^{II} is in the order of few μs, we can rule out the latter as

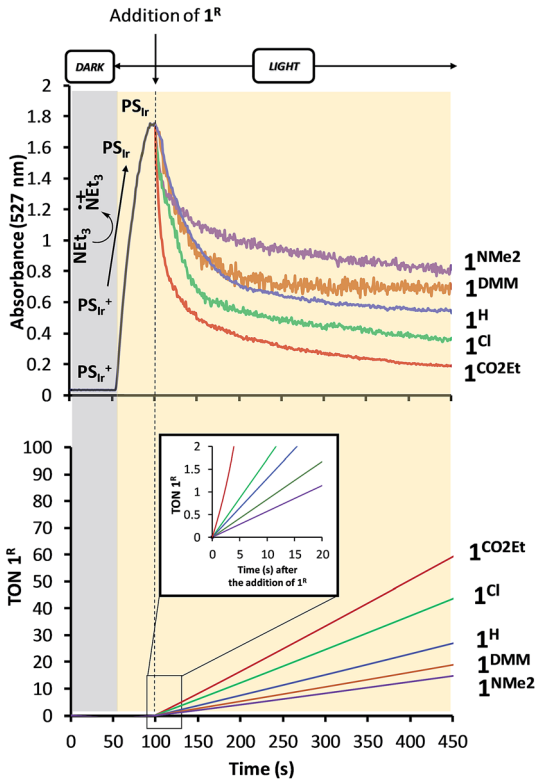

Fig. 8 (Top) UV-Vis spectral changes monitored at 527 nm associated with the formation of PS_{Ir} upon irradiation at $\lambda = 447$ nm and addition of 1^R complexes (0.1 eq. *vs.* PS_{Ir}^+). (Bottom) Time-dependent photocatalytic H_2 evolution. Inset: magnification of the H_2 evolution during the first seconds after addition of 1^R. Conditions: $[PS_{Ir}^+] = 0.25$ mM, $[Et_3N] = 100$ mM, $CH_3CN : H_2O$ (0.8 : 1.2 mL) at 25 °C.

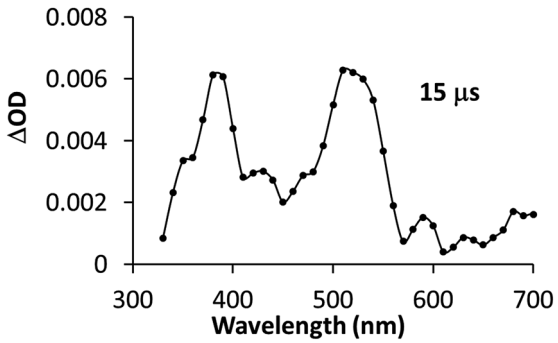

Fig. 9 Transient absorption spectrum of a solution containing PS_{Ir}^+ (50 μM), Et_3N (20 mM) and 1^{CO2Et} (80 μM) recorded at 15 μs after laser excitation. All measurements were carried out under N_2 at room temperature in acetonitrile ($\lambda_{ex} = 355$ nm, $E = 8$ mJ per pulse).

the rate-determining step of the catalytic cycle (a TOF = 14.4 s^{-1}, corresponding to 70 ms per cycle, was obtained for 1^{CO2Et}).

Kinetic Isotope Effect (KIE). KIE studies on the reaction rate ($KIE^g = k_{H_2O}/k_{D_2O}$) as well as the isotopic distribution ($H_2 : HD : D_2$) analysis were carried out to better understand the protonation steps in the catalytic cycle (see Scheme 1, see Section ESI 7† for Experimental details). The on-line monitoring of the isotopic distribution can provide information not only about the rate-determining step but also about the hydrogen–hydrogen bond formation step. Nevertheless, a study of the formation rate of the different isotopomers (H_2, HD and D_2) and isotopic ratios has never been performed in the context of photocatalytic water reduction.

Studies were performed in H_2O, D_2O (99%) and $H_2O : D_2O$ (1 : 1) using 1^H as catalyst (Fig. 10 and S35†). The KIE^g (k_{H_2O}/k_{D_2O}) value, obtained by comparing the initial reactions rates in H_2O *vs.* D_2O (99.9%), was 2.5 (Fig. S36†). This suggests that the rate-determining step of the overall catalytic process could involve a formation of a X–H bond, such as the protonation of Co^I or Co^{II}–H intermediates, to give Co^{III}–H or hydrogen, respectively.[27] On-line MS studies provided further insights into the identification of the specific products generated during the light-driven catalysed processes (Fig. 10).

Irradiation of 1^H in D_2O resulted in a constant isotopic distribution of 0.5% H_2, 9.1% HD and 90.4% D_2 throughout all the experiment (Fig. S32†), which is an indication that the mechanism does not change over the reaction time. The HD and H_2 measured should be attributed to the H_2O content (1%) in D_2O, which indicates a large isotopic selectivity. Likewise, when using a $H_2O : D_2O$ (1 : 1) mixture the isotopic distribution was H_2 (68.2 ± 0.2%) > HD (29.3 ± 0.2%) ≫ D_2 (2.6 ± 0.2%) (Fig. 10), again unmodified during the reaction profile. The isotopic selectivity, H_2 *vs.* HD ($KIE^{Sel}(H_2/HD)$), is 2.3 (these two isotopomers are > 97% of the evolved gas), very close to the KIE^g of 2.5. This suggests a coincidence in the rate-determining step and the reaction step that affects the H_2/HD distribution. Moreover, the 26.6 ± 0.5 and 11.5 ± 0.1 values for the H_2/D_2 ($KIE^{Sel}(H_2/D_2)$) and HD/D_2 ($KIE^{Sel}(HD/D_2)$) ratios, respectively, are in agreement with two consecutive protonation events.

Presumably, the two consecutive events that control the isotopic distribution are the cobalt hydride bond formation and the hydrogen–hydrogen bond formation (see Fig. 10), but only the first affects the reaction rate. This is in agreement with the cobalt protonation as the rate-determining step of the hydrogen evolution.

Mechanistic discussion

To further evaluate the impact of the electronic effects on the $Co^{II/I}$ redox and the Co^I protonation in the reaction rate we have computationally studied the thermodynamics of these elemental steps for all 1^R complexes. We performed computational studies at the B3LYP-D_3/cc-pVTZ//B3LYP-D_3/6-31+G* level of theory, which previously gave good agreement in similar catalytic systems (see ESI† for Computational details).[28] Theoretical $E_{1/2}(Co^{II/I})$ and $E_{1/2}(Co^{III/II})$ values correlate within the expected errors for all 1^R complexes (see Table 2). We also computed the Co^{III}–H pK_a values, which are in the range from 8.4 to 15.4.

Our experimental studies discard that only the PS_{Ir} to Co^{II} electron transfer step determines the rate of the overall process since it is much faster than the TOF. Therefore should be influence also by a second step. Indeed, the calculated difference of $Co^{II/I}$ reduction potential between 1^{NMe2} and 1^{CN} is 330 mV, corresponding to −7.5 kcal mol^{-1} (expt. 380 mV,

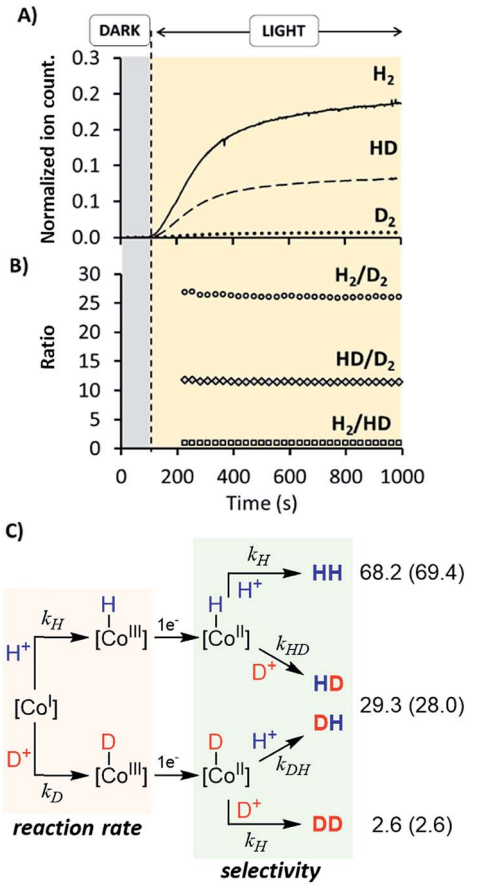

Fig. 10 (A) On-line monitoring of H_2 (solid trace), HD (dashed trace) and D_2 (dotted line) formation *vs.* time in a MeCN : H_2O : D_2O (0.8 : 0.6 : 0.6 mL) solvent mixture. (B) Ratios of H_2/D_2 (dots), HD/D_2 (diamonds) and H_2/HD (squares) obtained from the ion current data. Conditions: $\mathbf{1}^{H}$ (50 μM), PS_{Ir}^{+} (150 μM), MeCN : H_2O : D_2O (0.8 : 0.6 : 0.6 mL), Et_3N (40 μL), reaction volume = 2 mL, irradiated at λ = 447 nm, under N_2 atmosphere. Ion current response was calibrated with HD and D_2 authentic samples. (C) Heterolytic mechanism for the formation of isotopic distribution of H_2, DH and D_2. In parenthesis are the theoretical calculated values.

-8.9 kcal mol^{-1}). These energies reflect the experimentally observed trend for catalysis, *i.e.* higher the $E_{1/2}(Co^{II/I})$ reduction potential faster the hydrogen evolution catalysis. However, taking into account only the $E_{1/2}(Co^{II/I})$ values, the reaction rate should be *ca.* 3×10^7 times faster for $\mathbf{1}^{CN}$ than $\mathbf{1}^{NMe2}$ (considering the experimental $E_{1/2}(Co^{II/I})$, 3×10^6 considering the theoretical values). However, the experimental rate increase between $\mathbf{1}^{NMe2}$ and $\mathbf{1}^{CN}$ is only about 20-fold (-1.8 kcal mol^{-1}), approximately 6 orders of magnitude different. We can also rule out the Co^{I} protonation to form Co^{III}–H as the only contribution to the rate law. The Co^{III}–H pK_a values difference between $\mathbf{1}^{NMe2}$ and $\mathbf{1}^{CN}$ corresponds to +9.5 kcal mol^{-1}, which is opposite to the redox values. In this scenario and considering the Bell–Evans–Polanyi (BEP) principle and Marcus type analytical expressions (1–3) (see below), lower the pK_a of Co^{III}–H species, slower the catalytic reaction rate.

Therefore, the energy barrier of the reaction either involves a stepwise Co^{II} reduction followed by protonation (rate-determining step suggested by KIE), or a proton coupled electron transfer (CPET). However, based on thermodynamic data, BEP and eqn (1)–(3), we may discard both possible CPET, $Co^{II} \rightarrow Co^{III}$–H and $Co^{I} \rightarrow Co^{II}$–H, as they are +3.5 and +5.5 kcal mol^{-1} less favourable for $\mathbf{1}^{CN}$ than for $\mathbf{1}^{NMe2}$, respectively.[29] Thus, neither $CPET_1$ nor $CPET_2$ processes can be involved in the rate-determining step.

We have also calculated the protonation barrier for Co^{I}, in both cases $\mathbf{1}^{H}$ and $\mathbf{1}^{CO2Et}$, being the $\Delta\Delta G^{\ddagger}$ value 3.2 kcal mol^{-1} in favour of $\mathbf{1}^{H}$, again opposite to the energy obtained from the experimental results (-0.8 kcal mol^{-1}). Finally, we have considered the sum of the $Co^{II/I}$ reduction potential thermodynamics and the energy barrier for the Co^{I} protonation. This is indeed the value of the total energy barrier if the production of Co^{I} is an endergonic step (see Fig. 11). In this case, the difference between the $\mathbf{1}^{H}$ and $\mathbf{1}^{CO2Et}$ energy barriers is -1.0 kcal mol^{-1}, which is in very good agreement with the experimental energy difference (-0.8 kcal mol^{-1}). Calculated kinetic isotopic effects for this mechanism for $\mathbf{1}^{H}$ (3.8) qualitatively matches with the experimental KIE^{g} (k_{H_2O}/k_{D_2O}) of 2.5. The KIEs values calculated starting from Co–H and Co–D, to give hydrogen, are 7.1 and 6.9, respectively, which are clearly much larger than the experimental KIE^{g} (k_{H_2O}/k_{D_2O}). In addition, we have calculated the distribution of the isotopomers using the values obtained theoretically and considering the proposed mechanism (Fig. 11). Interestingly, the experimental and theoretical isotopic distributions matched perfectly (experimental [H_2: 68.2, HD: 29.3, D_2: 2.6] and Theoretical [H_2: 69.1, HD: 28.3, D_2 2.6]) (see Fig. S10c†).

At this point it is interesting to discuss this result within the context of the theoretical model developed by M. Koper and co.,[30] which takes into account the role of the pH in the selectivity between the concerted proton–electron transfer (CPET) and sequential proton–electron (or electron-proton) transfer (SPET) pathways. The proposed theoretical model assumes an outer-sphere charge transfer mechanism and provides the following Marcus-type analytical expressions for the activation

Table 2 Theoretical reduction potential, pK_a and CPET reduction potential values for $\mathbf{1}^{R}$ computed at B3LYP-D_3/cc-pVTZ//B3LYP-D3/6-31+G* level

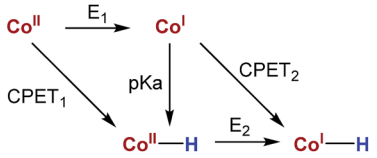

Complex	$E_1{}^{a}$ (V)	$E_2{}^{a}$ (V)	pK_a	$CPET_1{}^{a,b}$ (V)	$CPET_2{}^{a,b}$ (V)
$\mathbf{1}^{NMe2}$	−1.92	−1.53	15.4	−1.69	−1.27
$\mathbf{1}^{DMM}$	−1.92	−1.49	14.7	−1.73	−1.27
$\mathbf{1}^{H}$	−1.85	−1.46	12.9	−1.75	−1.35
$\mathbf{1}^{Cl}$	−1.82	−1.42	11.9	−1.80	−1.36
$\mathbf{1}^{COOEt}$	−1.74	−1.44	11.5	−1.80	−1.40
$\mathbf{1}^{CN}$	−1.59	−1.36	8.4	−1.84	−1.51

[a] *vs.* $Fc^{+/0}$ [b] The CPET reduction potential values have been adjusted to pH = 11.

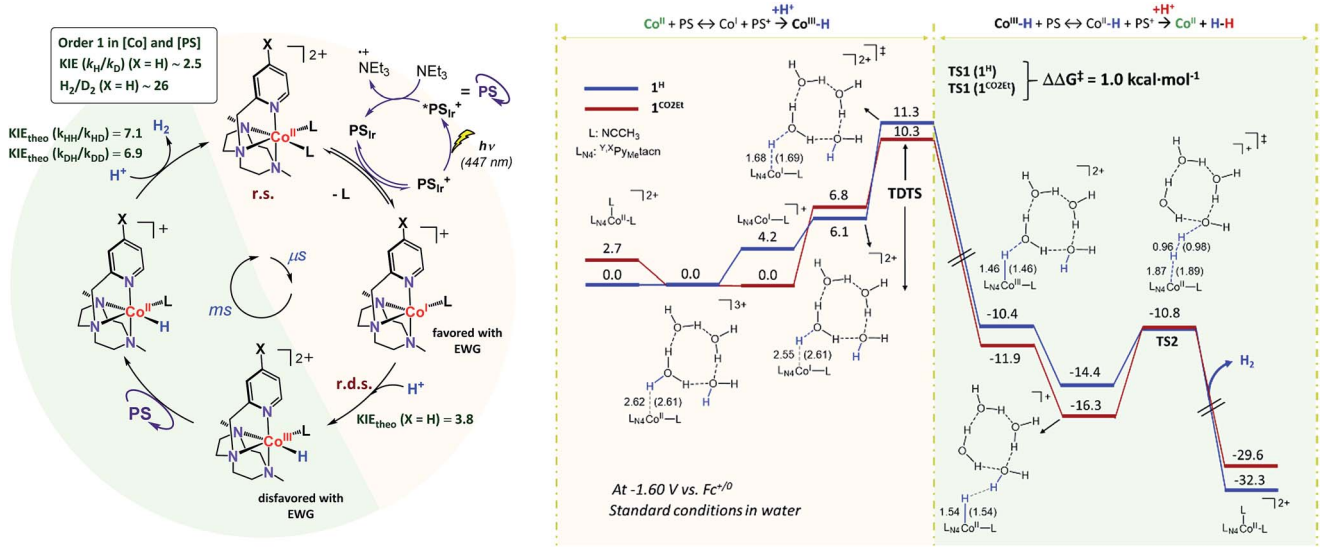

Fig. 11 (Left) Proposed mechanism for H_2 evolution catalysed by $\mathbf{1}^{R}$ complexes. (Right) values are ΔG. Energies are given in kcal mol^{-1}. B3LYP-D_3/aug-cc-pVTZ(-f)//B3LYP-D_3/6-31+G* level of theory. Bond lengths for $\mathbf{1}^{H}$ ($\mathbf{1}^{COOEt}$) are shown in Armstrongs.

energies of the electron-transfer (ET), proton transfer (PT) and CPET steps.

$$k_{ET} = k^0_{ET} \exp\left(- \frac{(\lambda_{ET} + \Delta G_{ET})^2}{4\lambda_{ET} RT} \right) \quad (1)$$

$$k_{PT} = k^0_{PT} \exp\left(- \frac{(\lambda_{PT} + \Delta G_{PT})^2}{4\lambda_{PT} RT} \right) \quad (2)$$

$$k_{CPET} = k^0_{CPET} \exp\left(- \frac{(\lambda_{CPET} + \Delta G_{CPET})^2}{4\lambda_{CPET} RT} \right) \quad (3)$$

$$\lambda_{CPET} = \lambda_{ET} + \lambda_{PT} + 2\lambda \quad (4)$$

where λ_x and ΔG_x are the reorganization and reaction free energies, respectively. Eqn (1)–(3) illustrate that in this model: (i) the thermodynamics proportionally affects kinetics (*via* the ΔG term); (ii) the thermodynamics and kinetics for ET, PT and CPET scale differently with pH. As described by the M. Koper's model, considering $\lambda = 0$ (estimated by Hammes-Schiffer *et al.*),[31] and equivalent pre-exponential factors (k°), when $\lambda_{CPET} \approx \lambda_{ET}$ the transition between CPET and SPET is around pH $\approx$ pK_a (pK_a correspond to the protonation step). The transition spans approximately a pH range of ± 2 in which both CPET and SPET mechanisms are competitive. When the pH > (pK_a + 2) purely SPET is proposed. In our case, the pH of the reaction media it is fixed at around 11.4, due to the reaction conditions (Et_3N 2% v/v) and it does not substantially modify during the reaction. Interestingly, our catalytic system has a pK_a span from 8.4 to 15.4 (Table 2), crossing the pH value of the solution. However, there are clear evidences that reaction mechanism does not change with the ligand substituents as judged by the Hammett plot (Fig. 4). For the presented catalysts we propose a scenario where $\lambda_{CPET} > \lambda_{ET}$, as expected by eqn (4), and the position of the transition region is shifted to lower pH, in agreement with our observations.

Altogether, our results are in agreement with a sequential reduction-protonation mechanism (SEP), in which the Co^{I} protonation, to give Co^{III}–H, determines the TOF-dependent transition state (TDTS).[32] Furthermore, in the proposed catalytic cycle the TOF-determining intermediate (TDI) is dependent on the redox potentials of either the photosensitizer ($E_{1/2}(\mathbf{PS_{Ir}}^{+/0})$) and the starting Co^{II} complex ($E_{1/2}(Co^{II/I})$). In our case, from combined UV-Vis spectroscopic/H_2 evolution monitoring studies, we have observed that the concentration of photosensitizer in the reduced form is very low. Therefore, the $E_{1/2}$ redox potential of the photosensitizer should be used only as an estimation. Considering the Nernst equation and the concentration of the photosensitizer species in solution, we can roughly estimate that the redox potential of the $\mathbf{PS_{Ir}}^{+/0}$ couple is about 100–200 mV less reducing that the $E_{1/2}$. Accordingly, the redox potential for $Co^{II/I}$ should be more reducing than the photosensitizer. The difference in redox potential between the $Co^{II/I}$ and photosensitize is directly translate in the hydrogen evolution reaction rate becoming faster with a more electron-withdrawing ligand. In other words, Co^{II} is the TOF-determining intermediate and its reduction is an endergonic step that contributes to increase the total energy barrier (see Fig. 11). On the other hand, if the redox potential of the photosensitizer is more reducing (lower $E(Co^{II/I})$ reduction potential)[33] that redox potential of the $Co^{II/I}$ process, the rate could be only dependent on the Co^{I} protonation, which is expected to be thermodynamically less feasible for more electron-withdrawing ligands (see Table 2). This simplified scenario may help to rationalize some of the different results in the field of light-driven water reduction (Fig. 12).

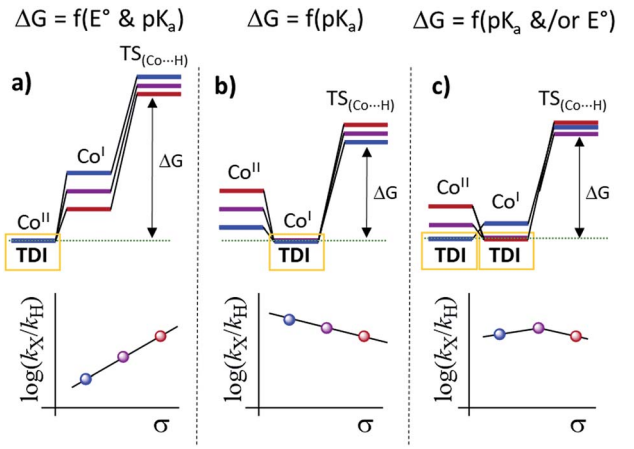

Fig. 12 Simplified mechanism scenarios from the Co^{II} species to the Co^{I} protonation transition state and related Hammett plots considering the electronic effects in hypothetical situations regarding the reducing redox potentials of $PS^{n/n-1}$ (photosensitizer) and $Co^{II/I}$ couples. (a) $E_{1/2}(Co^{II/I})$ value is substantially more reducing than $E(PS^{n/n-1})$, (b) $E(PS^{n/n-1})$ value is substantially more reducing than $E_{1/2}(Co^{II/I})$, (c) $E(PS^{n/n-1})$ value is intermediate in the $E_{1/2}(Co^{II/I})$ series.

Conclusions

We have developed a new family of cobalt complexes active for water reduction, which allows for a systematic study of the catalytic activity as a function of the electronic properties of the metal centre. Within the series, a span of 380 mV for the $E_{1/2}(Co^{II/I})$ resulted in 20-fold increase of H_2 evolution activity, by modification of the pyridine substituents (from the electron-donating $-NMe_2$, to the electron-withdrawing –CN group). UV-Vis spectroscopy, Luminescence Quenching Studies and Transient Absorption Spectroscopy, allow to study the reaction of photogenerated $[Ir^{III}(ppy)_2(bpy^{\bullet-})]$ ($\mathbf{PS_{Ir}}$) species with the different Co^{II} complexes to form the elusive Co^{I} intermediates. Formation of the Co^{I} is estimated to be in the order of μs, much faster that the catalytic rate. Kinetic isotopic experiments together with DFT calculations are consistent with: (i) the Co^{I} protonation to form Co^{III}–H as the TOF-determining transition state (TDTS) of the catalytic cycle and (ii) Co^{II} species as the TOF-determining intermediate (TDI). We propose that in the herein reported catalytic system (under basic conditions), the TDI depends on the redox potentials of both $\mathbf{1^R}$ metal complexes and photoredox catalysts. We postulate that these phenomena could be more general. Ongoing work in our group is tackling this problem. We envision that the reported mechanistic investigation will aid in the general understanding of the water reduction reaction, and will trigger the development of more active water reduction catalysts.

Conflicts of interest

There are no conflicts to declare.

Acknowledgements

We would like to thank the European Commission for the ERC-CG-2014-648304 (J. Ll.-F.) project and Spanish MINECO (CTQ2016-80038-R) project. The financial support from ICIQ Foundation and CELLEX Foundation through the CELLEX-ICIQ high throughput experimentation platform and the Starting Career Program is gratefully acknowledged. We also thank CERCA Programme (Generalitat de Catalunya); The MINECO is acknowledged for a FPU fellowship to A. C. (AP2012-6436) and ICIQ-IPMP program (F. F.) and Severo Ochoa Excellence Accreditation 2014–2018 (SEV-2013-0319). J. M. L. is grateful for financial support from the Spanish MINECO CTQ2014-52525-P and the Catalan DIUE 2014SGR931. J. P.-P. gratefully acknowledge CTQ2014-60174-P (partially co-financed with FEDER funds), Maria de Maeztu (MDM-2015-0538), (RyC contract to MGB) and Fundación Ramón Areces for financial support. We also thank Catexel for a generous gift of tritosyl-1,4,7-triazacyclononane.

Notes and references

1 (*a*) H. B. Gray, *Nat. Chem.*, 2009, **1**, 7; (*b*) N. S. Lewis and D. G. Nocera, *Proc. Natl. Acad. Sci. U. S. A.*, 2006, **103**, 15729.

2 (*a*) P. Du and R. Eisenberg, *Energy Environ. Sci.*, 2012, **5**, 6012; (*b*) J. R. McKone, S. C. Marinescu, B. S. Brunschwig, J. R. Winkler and H. B. Gray, *Chem. Sci.*, 2014, **5**, 865; (*c*) V. Artero, M. Chavarot-Kerlidou and M. Fontecave, *Angew. Chem., Int. Ed.*, 2011, **50**, 7238.

3 (*a*) A. Kahnt, K. Peuntinger, C. Dammann, T. Drewello, R. Hermann, S. Naumov, B. Abel and D. M. Guldi, *J. Phys. Chem. A*, 2014, **118**, 4382; (*b*) S. C. Marinescu, J. R. Winkler and H. B. Gray, *Proc. Natl. Acad. Sci. U. S. A.*, 2012, **109**, 15127–15131; (*c*) D. Moonshiram, C. Gimbert-Surinach, A. Guda, A. Picon, C. S. Lehmann, X. Zhang, G. Doumy, A. M. March, J. Benet-Buchholz, A. Soldatov, A. Llobet and S. H. Southworth, *J. Am. Chem. Soc.*, 2016, **138**, 10586; (*d*) D. C. Lacy, G. M. Roberts and J. C. Peters, *J. Am. Chem. Soc.*, 2015, **137**, 4860; (*e*) A. Bhattacharjee, M. Chavarot-Kerlidou, E. S. Andreiadis, M. Fontecave, M. J. Field and V. Artero, *Inorg. Chem.*, 2012, **51**, 7087.

4 (*a*) N. Queyriaux, R. T. Jane, J. Massin, V. Artero and M. Chavarot-Kerlidou, *Coord. Chem. Rev.*, 2015, **304–305**, 3; (*b*) W. K. Lo, C. E. Castillo, R. Gueret, J. Fortage, M. Rebarz, M. Sliwa, F. Thomas, C. J. McAdam, G. B. Jameson, D. A. McMorran, J. D. Crowley, M. N. Collomb and A. G. Blackman, *Inorg. Chem.*, 2016, **55**, 4564; (*c*) B. Shan, T. Baine, X. A. Ma, X. Zhao and R. H. Schmehl, *Inorg. Chem.*, 2013, **52**, 4853; (*d*) S. Varma, C. E. Castillo, T. Stoll, J. Fortage, A. G. Blackman, F. Molton, A. Deronzier and M. N. Collomb, *Phys. Chem. Chem. Phys.*, 2013, **15**, 17544.

5 B. H. Solis and S. Hammes-Schiffer, *J. Am. Chem. Soc.*, 2011, **133**, 19036.

6 (*a*) A. Lewandowska-Andralojc, T. Baine, X. Zhao, J. T. Muckerman, E. Fujita and D. E. Polyansky, *Inorg. Chem.*, 2015, **54**, 4310; (*b*) A. Rodenberg, M. Orazietti, B. Probst, C. Bachmann, R. Alberto, K. K. Baldridge and

P. Hamm, *Inorg. Chem.*, 2015, **54**, 646; (*c*) W. M. Singh, M. Mirmohades, R. T. Jane, T. A. White, L. Hammarstrom, A. Thapper, R. Lomoth and S. Ott, *Chem. Commun.*, 2013, **49**, 8638; (*d*) S. Mandal, S. Shikano, Y. Yamada, Y. M. Lee, W. Nam, A. Llobet and S. Fukuzumi, *J. Am. Chem. Soc.*, 2013, **135**, 15294.

7 A. Call, Z. Codolà, F. Acuña-Parés and J. Lloret-Fillol, *Chem.–Eur. J.*, 2014, **20**, 6171.

8 (*a*) P. Du, J. Schneider, G. Luo, W. W. Brennessel and R. Eisenberg, *Inorg. Chem.*, 2009, **48**, 4952; (*b*) U. J. Kilgore, J. A. Roberts, D. H. Pool, A. M. Appel, M. P. Stewart, M. R. DuBois, W. G. Dougherty, W. S. Kassel, R. M. Bullock and D. L. DuBois, *J. Am. Chem. Soc.*, 2011, **133**, 5861; (*c*) U. J. Kilgore, M. P. Stewart, M. L. Helm, W. G. Dougherty, W. S. Kassel, M. R. DuBois, D. L. DuBois and R. M. Bullock, *Inorg. Chem.*, 2011, **50**, 10908; (*d*) D. L. DuBois, *Inorg. Chem.*, 2014, **53**, 3935; (*e*) B. H. Solis, Y. Yu and S. Hammes-Schiffer, *Inorg. Chem.*, 2013, **52**, 6994.

9 Y. Sun, J. Sun, J. R. Long, P. Yang and C. J. Chang, *Chem. Sci.*, 2013, **4**, 118.

10 (*a*) R. S. Khnayzer, V. S. Thoi, M. Nippe, A. E. King, J. W. Jurss, K. A. El Roz, J. R. Long, C. J. Chang and F. N. Castellano, *Energy Environ. Sci.*, 2014, **7**, 1477; (*b*) M. Nippe, R. S. Khnayzer, J. A. Panetier, D. Z. Zee, B. S. Olaiya, M. Head-Gordon, C. J. Chang, F. N. Castellano and J. R. Long, *Chem. Sci.*, 2013, **4**, 3934.

11 A. Mahammed, B. Mondal, A. Rana, A. Dey and Z. Gross, *Chem. Commun.*, 2014, **50**, 2725.

12 (*a*) J. Lloret-Fillol, Z. Codolà, I. Garcia-Bosch, L. Gómez, J. J. Pla and M. Costas, *Nat. Chem.*, 2011, **3**, 807; (*b*) I. Prat, D. Font, A. Company, K. Junge, X. Ribas, M. Beller and M. Costas, *Adv. Synth. Catal.*, 2013, **355**, 947; (*c*) I. Garcia-Bosch, Z. Codola, I. Prat, X. Ribas, J. Lloret-Fillol and M. Costas, *Chem.–Eur. J.*, 2012, **18**, 13269; (*d*) I. Prat, A. Company, T. Corona, T. Parella, X. Ribas and M. Costas, *Inorg. Chem.*, 2013, **52**, 9229; (*e*) A. Company, L. Gomez, X. Fontrodona, X. Ribas and M. Costas, *Chem.–Eur. J.*, 2008, **14**, 5727; (*f*) A. Company, L. Gómez, M. Güell, X. Ribas, J. M. Luis, J. Lawrence Que and M. Costas, *J. Am. Chem. Soc.*, 2007, **129**, 15766.

13 A. L. Ward, L. Elbaz, J. B. Kerr and J. Arnold, *Inorg. Chem.*, 2012, **51**, 4694–4706.

14 C. Hansch, A. Leo and R. W. Taft, *Chem. Rev.*, 1991, **91**, 165.

15 V. Artero and M. Fontecave, *Chem. Soc. Rev.*, 2013, **42**, 2338.

16 C. Bachmann, M. Guttentag, B. Spingler and R. Alberto, *Inorg. Chem.*, 2013, **52**, 6055.

17 (*a*) M. Guttentag, A. Rodenberg, C. Bachmann, A. Senn, P. Hamm and R. Alberto, *Dalton Trans.*, 2013, **42**, 334; (*b*) W. M. Singh, T. Baine, S. Kudo, S. Tian, X. A. Ma, H. Zhou, N. J. DeYonker, T. C. Pham, J. C. Bollinger, D. L. Baker, B. Yan, C. E. Webster and X. Zhao, *Angew. Chem., Int. Ed.*, 2012, **51**, 5941; (*c*) E. Joliat, S. Schnidrig, B. Probst, C. Bachmann, B. Spingler, K. K. Baldridge, F. von Rohr, A. Schilling and R. Alberto, *Dalton Trans.*, 2016, **45**, 1737.

18 C. Bachmann, B. Probst, M. Guttentag and R. Alberto, *Chem. Commun.*, 2014, **50**, 6737.

19 R. S. Khnayzer, V. S. Thoi, M. Nippe, A. E. King, J. W. Jurss, K. A. El Roz, J. R. Long, C. J. Chang and F. N. Castellano, *Energy Environ. Sci.*, 2014, **7**, 1477.

20 (*a*) J. W. Jurss, R. S. Khnayzer, J. A. Panetier, K. A. El Roz, E. M. Nichols, M. Head-Gordon, J. R. Long, F. N. Castellano and C. J. Chang, *Chem. Sci.*, 2015, **6**, 4954; (*b*) M. Nippe, R. S. Khnayzer, J. A. Panetier, D. Z. Zee, B. S. Olaiya, M. Head-Gordon, C. J. Chang, F. N. Castellano and J. R. Long, *Chem. Sci.*, 2013, **4**, 3934.

21 (*a*) H. Lv, W. Guo, K. Wu, Z. Chen, J. Bacsa, D. G. Musaev, Y. V. Geletii, S. M. Lauinger, T. Lian and C. L. Hill, *J. Am. Chem. Soc.*, 2014, **136**, 14015; (*b*) A. Kobayashi, S. Watanabe, M. Ebina, M. Yoshida and M. Kato, *J. Photochem. Photobiol., A*, 2017, **347**, 9; (*c*) Y.-J. Yuan, Z.-T. Yu, X.-J. Liu, J.-G. Cai, Z.-J. Guan and Z.-G. Zou, *Sci. Rep.*, 2014, **4**, 4045; (*d*) J. I. Goldsmith, W. R. Hudson, M. S. Lowry, T. H. Anderson and S. Bernhard, *J. Am. Chem. Soc.*, 2005, **127**, 7502.

22 D. Hollmann, F. Gartner, R. Ludwig, E. Barsch, H. Junge, M. Blug, S. Hoch, M. Beller and A. Bruckner, *Angew. Chem., Int. Ed.*, 2011, **50**, 10246.

23 A. Panagiotopoulos, K. Ladomenou, D. Sun, V. Artero and A. G. Coutsolelos, *Dalton Trans.*, 2016, **45**, 6732.

24 (*a*) E. A. Plummer, J. W. Hofstraat and L. D. Cola, *Dalton Trans.*, 2003, 2080; (*b*) Y. You and W. Nam, *Chem. Soc. Rev.*, 2012, **41**, 7061; (*c*) J. Zhao, W. Wu, J. Sun and S. Guo, *Chem. Soc. Rev.*, 2013, **42**, 5323.

25 (*a*) S.-H. Wu, J.-W. Ling, S.-H. Lai, M.-J. Huang, C. H. Cheng and I.-C. Chen, *J. Phys. Chem. A*, 2010, **114**, 10339; (*b*) F. Garces, K. A. King and R. J. Watts, *Inorg. Chem.*, 1988, **27**, 3464; (*c*) D. Hanss, J. C. Freys, G. r. Bernardinelli and O. S. Wenger, *Eur. J. Inorg. Chem.*, 2009, **2009**, 4850; (*d*) M. S. Lowry and S. Bernhard, *Chem.–Eur. J.*, 2006, **12**, 7970.

26 (*a*) A. Rodenberg, M. Orazietti, B. Probst, C. Bachmann, R. Alberto, K. K. Baldridge and P. Hamm, *Inorg. Chem.*, 2015, **54**, 646; (*b*) M. Natali, *ACS Catal.*, 2017, **7**, 1330; (*c*) C.-F. Leung, S.-M. Ng, C.-C. Ko, W.-L. Man, J. Wu, L. Chen and T.-C. Lau, *Energy Environ. Sci.*, 2012, **5**, 7903; (*d*) A. Neubauer, G. Grell, A. Friedrich, S. I. Bokarev, P. Schwarzbach, F. Gärtner, A.-E. Surkus, H. Junge, M. Beller, O. Kühn and S. Lochbrunner, *J. Phys. Chem. Lett.*, 2014, **5**, 1355.

27 S. Aoi, K. Mase, K. Ohkubo and S. Fukuzumi, *Chem. Commun.*, 2015, **51**, 15145.

28 F. Acuña-Parés, Z. Codolà, M. Costas, J. M. Luis and J. Lloret-Fillol, *Chem.–Eur. J.*, 2014, **20**, 5696.

29 M. Bourrez, R. Steinmetz, S. Ott, F. Gloaguen and L. Hammarström, *Nat. Chem.*, 2015, **7**, 140.

30 (*a*) A. J. Göttle and M. T. M. Koper, *Chem. Sci.*, 2017, **8**, 458; (*b*) M. T. M. Koper, *Phys. Chem. Chem. Phys.*, 2013, **15**, 1399.

31 (*a*) B. Auer, A. V. Soudackov and S. Hammes-Schiffer, *J. Phys. Chem. B*, 2012, **116**, 7695; (*b*) S. Hammes-Schiffer, *ChemPhysChem*, 2002, **3**, 33; (*c*) S. Hammes-Schiffer and A. A. Stuchebrukhov, *Chem. Rev.*, 2010, **110**, 6939.

32 S. Kozuch and S. Shaik, *Acc. Chem. Res.*, 2011, **44**, 101.

33 The reduction redox potential is defined as the potential of a compound measured under standards conditions against a standard reference half-cell.